Genome wide identification and co-expression analysis of the xyloglucan endotransglucosylase/hydrolase gene family in Japanese morning glory

Kazuchika Yamauchi
Nagoya University
Katsuhiro Shiratake
shira@agr.nagoya-u.ac.jp

Nagoya University

Article

Keywords: co-expression network analysis, flower opening, genome-wide identification, Ipomoea nil, petal development, xyloglucan endotransglucosylase/hydrolase (XTH)

Posted Date: June 1st, 2026

DOI: https://doi.org/10.21203/rs.3.rs-9702690/v1

Additional Declarations: No competing interests reported.

Genome wide identification and co-expression analysis of the xyloglucan endotransglucosylase/hydrolase gene family in Japanese morning glory

Kazuchika Yamauchi and Katsuhiro Shiratake*

Graduate School of Bioagricultural Sciences, Nagoya University, Chikusa, Nagoya 464-8601, Japan

*Corresponding author : shira@agr.nagoya-u.ac.jp

Abstract

Flower opening is a dynamic process involving cell proliferation and turgor-mediated petal cell expansion. The xyloglucan endotransglucosylase/hydrolase (XTH) family enzymes are essential for these events, yet the functional roles and temporal deployment of this diverse gene family in ephemeral-flowering plant *Ipomoea nil* remains uncharacterized. In this study, 36 XTHs were identified, and their physicochemical properties and subcellular localizations were predicted, alongside organ-specific expression profiles. Furthermore, time-course transcriptomic data were utilized to

identify their specialized expression patterns through co-expression network analysis. This revealed that *InXTH* genes are organized into distinct modules synchronized with specific developmental stages. Specifically, two *InXTH* genes are highly active during the early cell-division phase, whereas five and one members are expressed immediately before and at flower opening, respectively. At these later stages, a single dominant isozyme exhibits exceptionally high transcript levels in each module, suggesting these dominant XTHs likely contribute to the cell wall remodeling required for anthesis. These findings provide fundamental insights into the temporal orchestration of cell wall-modifying enzymes and establish a molecular framework for understanding flower opening in dicots.

Keywords: co-expression network analysis, flower opening, genome-wide identification, *Ipomoea nil*, petal development, xyloglucan endotransglucosylase/hydrolase (XTH)

1. Introduction

Petal growth is initially driven by cell division and subsequently by extensive cell expansion [1]. Therefore, the rapid expansion of petal cells is a major determinant of flower size and morphology. This process is mediated by the accumulation of osmotic solutes,

including sugars and inorganic ions, in the vacuole, leading to an increase in intracellular osmotic potential and the consequent influx of water into the cell [2]. Simultaneously, cell wall loosening reduces the mechanical constraints on cell expansion, thereby allowing turgor-driven cell enlargement to proceed efficiently. As a result, petal cells undergo a substantial increase in volume during flower opening. Therefore, elucidating the molecular and physiological mechanisms regulating solute accumulation, cell wall modification, and water transport is essential for a comprehensive understanding of the flower-opening process.

At the cellular level, this turgor-driven expansion is constrained by the rigid cell wall. Mechanistically, intracellular turgor pressure drives irreversible extension of the primary cell wall, resulting in cell enlargement [3]. The primary cell wall is a composite network of cellulose microfibrils cross-linked by hemicellulosic polysaccharides, predominantly xyloglucans in dicotyledonous plants [3]. Therefore, controlled loosening of this cellulose-xyloglucan network is a prerequisite for irreversible wall extension under turgor pressure [4].

The xyloglucan endotransglucosylase/hydrolase (XTH) family plays a central role in this wall-remodeling process. XTHs catalyze endotransglucosylation (XET activity) and, in some isoforms, hydrolysis (XEH activity) of xyloglucan chains, thereby

55 modulating wall extensibility and mechanics [5-7]. *XTHs* form a large multigene family in
56 higher plants, and accumulating evidence indicates isoform-specific physicochemical
57 properties, subcellular localization, and developmental regulation [8-11]. Apart from petals,
58 XTHs are broadly implicated in primary cell wall remodeling during diverse
59 developmental stages, including primary root elongation [12], root hair initiation [13], and
60 fruit softening [14].

61 Cell expansion plays an important role in flowering, particularly in petal expansion.
62 While XTHs have been reported to participate in this process in several species, such as
63 carnation [15] and osmanthus [16], a systematic, genome-wide understanding of when and
64 which distinct XTH isoforms are deployed across high-resolution developmental time
65 courses is still limited.

66 Japanese morning glory (*Ipomoea nil*) has been cultivated as a traditional
67 horticultural plant in Japan for over four centuries. Scientifically, it has been used as a
68 model plant for studying photoperiodic flowering due to its high sensitivity to day length
69 [17], as well as for investigating flower color and morphology owing to its rich genetic
70 diversity [18]. In addition, extensive genetic and genomic resources for *I. nil* have been
71 developed and maintained through the National BioResource Project (NBRP) in Japan
72 (https://shigen.nig.ac.jp/asagao/index.jsp). Beyond these classical traits, *I. nil* is

characterized as an ephemeral “one-day flower,” where petal opening and senescence occur rapidly within a daily cycle [19]. The availability of the whole genome sequence [20], coupled with the recent acquisition of high-resolution time-course transcriptome data covering petal development from 72 hours before to 12 hours after flowering [21], provides a robust platform for molecular analysis. These extensive genomic resources, combined with their dramatic physiological changes, make *I. nil* an ideal model for dissecting the temporal regulation of cell wall-modifying enzymes during rapid organ expansion.

In this study, we performed a comprehensive genome-wide characterization of the *InXTH* gene family in *I. nil*, identifying 36 genes and analyzing their phylogenetics, chromosomal locations, and structural features. Furthermore, by applying weighted gene co-expression network analysis (WGCNA) to transcriptomic data in petals, we identified distinct gene modules corresponding to specific developmental stages. Our results suggest there is a stage-specific recruitment of distinct XTH isozymes, providing new insights into the transcriptional program orchestrating cell proliferation, rapid flower opening, and the subsequent senescence process.

2. Materials and methods

Identification of XTH genes in the Japanese morning glory genome

To identify the XTH gene candidates in Japanese morning glory (*Ipomoea nil*), BLASTP searches (e-value < 1e-10) were performed against the Japanese morning glory genome database (Asagao1.2 database, http://viewer.shigen.info/asagao/) [20] and the NCBI GenBank database. The amino acid sequences of *Arabidopsis thaliana* XTHs from TAIR (https://www.arabidopsis.org/) [22] were used as queries.

The retrieved sequences and gene IDs from both databases were cross-referenced. To address potential annotation errors or discrepancies observed in several genes, the coding sequences were curated by comparing the genomic sequences with RNA-seq data and by aligning the sequences from the two databases. These sequences were defined as the putative full-length sequences of *InXTHs* for further study.

To verify the protein classification, the presence of the Glyco_hydro_16 domain (PF00722) was confirmed using the InterProScan (https://www.ebi.ac.uk/interpro/) [23] against the Pfam database [24].

Physicochemical property and subcellular localization analysis

The basic physicochemical properties of the identified InXTH proteins, including the amino acid length, molecular weight (MW), isoelectric point (pI), and grand average of hydropathy (GRAVY), were predicted using the ProtParam tool on the ExPASy server (https://web.expasy.org/protparam/). For subcellular localization analysis, the presence of

N-terminal signal peptides and their cleavage sites were predicted using SignalP 6.0 (https://services.healthtech.dtu.dk/services/SignalP-6.0/) [25] with the "Eukarya" setting. TargetP 2.0 (https://services.healthtech.dtu.dk/services/TargetP-2.0/) [26] with the “Plant” organism group setting was used to discriminate between secretory pathway signal peptides, mitochondrial transit peptides, and chloroplast transit peptides. The precise subcellular location was predicted using DeepLoc 2.1 (https://services.healthtech.dtu.dk/services/DeepLoc-2.1/) [27].

Multiple sequence alignment and phylogenetic analysis

The amino acid sequences of XTHs were aligned using the CLUSTALW program(https://www.genome.jp/tools-bin/clustalw), and neighbor-joining (NJ) phylogenetic tree was constructed using MEGA12 [28] with the following parameters: Poisson model, pairwise deletion and 1,000 bootstrap replications. The identified XTHs were categorized into three subfamilies (Groups I/II, IIIA, IIIB) based on *Arabidopsis thaliana* [10] and *Ipomoea batatas* [11].

Gene structure and protein motif analysis

Gene structure (exon-intron structure) was schematized using coding sequences (CDSs) and genomic sequence of the *InXTH*s by the Gene Structure Display Server 2.0 (https://gsds.gao-lab.org/) [29]. Multiple Expectation Maximization for Motif Elicitation

(https://meme-suite.org/meme/tools/meme) [30] was used to identify the conserved motifs in the amino acid sequences of InXTHs. The parameters were set as follows: The "zero or one occurrence per sequence" (ZOOPS) model was selected for site distribution, the maximum number of motifs was set to 12, and the motif width was restricted to a range of 6 to 50 amino acids.

Chromosomal location and gene duplication analysis

Information regarding the chromosome distribution of the *InXTH* genes was retrieved from the Asagao1.2 database. The chromosomal locations were visualized using MapChart [31]. Tandemly duplicated genes were identified as clusters of two or more *InXTH* genes located within 100 kbp of each other.

Gene expression profile

Gene expression data for different organs of Japanese morning glory, expressed as RPKM values, were obtained from the Japanese morning glory RNA-seq database (https://viewer.shigen.info/asagao/download.php).

Prior to analysis, the expression values for *InXTH29*, which was annotated as two separate genes due to an annotation error, were corrected by calculating the length-weighted average of the RPKM values to represent the expression of the single full-length gene. For visualization, the RPKM values were log2-transformed [log2(RPKM + 1)] and

145 a heatmap was generated using the pheatmap R package, with hierarchical clustering
146 applied to the genes based on expression similarity.

147 Temporal gene expression data using FPKM values in petals were obtained from
148 the temporal transcriptome data and interactive database
149 (https://ipomoeanil.nibb.ac.jp/fpkm/) [21], which includes time-course transcriptome data
150 of petals at multiple stages, ranging from the pre-opening stage to the late senescence
151 stage.

152 **Weighted gene co-expression network construction analysis (WGCNA)**

153 For the construction of the co-expression network, the comprehensive FPKM
154 dataset derived from *Ipomoea nil* petals was downloaded from the DNA Data Bank of
155 Japan (DDBJ)/GEA under accession number E-GEAD-856 [21].

156 Co-expression network analysis was performed using WGCNA R package [32]. To
157 construct a robust scale-free network, we selected top 7,000 genes based on the coefficient
158 of variation of expression among all samples. In addition, 32 *InXTH* genes with detectable
159 expressions were explicitly included in the dataset, resulting in a total of 7,023 genes for
160 network construction. Soft-thresholding power of $\beta = 5$ was chosen to achieve a scale-
161 free topology fit index of 0.9. A signed network was constructed using the
162 blockwiseModules function, with a minimum module size of 30 and a merged cut height

of 0.25. Module membership (kME) was calculated for each *InXTH* gene as the correlation between its expression profile and the module eigengene of its assigned module. *InXTH* genes with kME < 0.3 were excluded from module-based analyses (n = 9), as they lacked reliable co-expression patterns.

Visualization of module expression profile and *InXTH* gene expression

To visualize the temporal expression patterns of each module, the mean Module Eigengene (ME) values were plotted across time points with standard errors. The expression level of *InXTH* genes within each module were evaluated using the maximum FPKM value observed within the entire time course. The values were visualized as bar plots, and pseudo-log10 transformation was applied to the y-axis to accommodate the expression levels using the ggplot2 R package.

3. Results

Identification and phylogenetic analysis of XTH genes in Japanese morning glory

To identify the *XTH* genes of Japanese morning glory, we performed a BLASTP search on the morning glory genome database (Asagao1.2 database, http://viewer.shigen.info/asagao/) [20] and the NCBI GenBank database, using amino acid sequences of *Arabidopsis thaliana* XTHs obtained from TAIR

(https://www.arabidopsis.org/) [22] as queries. In total, 37 and 42 candidates were identified in the Asagao1.2 database and the NCBI GenBank database, respectively (Supplemental Table S1, S2). Cross-reference of these candidates revealed several discrepancies from annotation differences between the two databases. Regarding splicing variants, XM_019343467.1 and XM_019343468.1 in the NCBI GenBank database were identified as identical to INIL12g22043 in the Asagao1.2 database. XM_019300959.1 and XM_019300960.1 were identified to be identical to INIL15g28182. Similarly, three splicing variants XM_019326605.1, XM_019326606.1, and XM_019326607.1 were found for INIL13g09293. The longest isoform, XM_019326605.1, was selected as the representative sequence. Furthermore, XM_019337944.1 and XM_019337945.1 both aligned to the exon regions of INIL03g17598, indicating potential redundancy in the GenBank database. Conversely, INIL03g17601 lacked a corresponding annotation in the NCBI GenBank database. For INIL13g15562, three amino acids deletion was observed after residue 62 in the Asagao1.2 sequence. The deletion was manually curated based on the orthologous sequence from sweet potato (*Ipomoea batatas*). Finally, comparison with a single locus XM_019332083.1 revealed that INIL12g01243 and INIL12g01244 each represent a fragment of a single locus, while annotated as two separate genes. Therefore, the sequence from XM_019332083.1 was used for further study. A total of 36 InXTHs,

including the previously reported InXTH1 to InXTH4 [33], were identified (Table 1). The newly identified XTHs were named InXTH5 to InXTH36, according to their gene position on the chromosomes. All 36 InXTH proteins were confirmed to possess the Glyco_hydro_16 domain (PF00722) by InterProScan (https://www.ebi.ac.uk/interpro/) [23] analysis against the Pfam database [24]. This domain belongs to the glycoside hydrolase family 16 (GH16) and serves as the core catalytic domain, containing the conserved motif essential for xyloglucan endotransglucosylase and hydrolase activities [34]. Furthermore, 35 of these proteins were also found to possess the xyloglucan endotransglucosylase (XET) C-terminus domain (PF06955).

Gene Name	Gene ID (Asagao1.2)	Gnomon (NCBI)	Sub family	Chromosome number	Position on chromosome		Strand	Source	Number of animo acids	Number of exons	Pfam ID	Molecular weight (Da)	pI	GRAVY	SignalP 6.0			TargetP 2.0	DeepLoc 2.1
					start	end									Prediction	Probability	Cleavage Site		
lnXTH1	INIL10g13325	XM_019330562.1	I/II	10	11,696,949	11,700,497	-	Asagao	295	4	PF00722, PF06955	34,031	8.8	-0.348	Sec/SPI	0.9998	21-22	Signal Peptide	Extracellular (0.70)
lnXTH2	INIL00g00888	XM_019328032.1	I/II	scaffold0177	202,039	204,229	-	Asagao	293	3	PF00722, PF06955	32,516	6.2	-0.323	Sec/SPI	0.9994	32-33	Signal Peptide	Extracellular (0.73)
lnXTH3	INIL12g07349	XM_019324453.1	I/II	12	13,998,009	13,999,624	-	NCBI	281	3	PF00722, PF06955	32,332	9.3	-0.350	Sec/SPI	0.9997	29-30	Signal Peptide	Extracellular (0.70)
lnXTH4	INIL02g40690	XM_019317605.1	I/II	2	9,532,946	9,534,570	+	Asagao	292	4	PF00722, PF06955	33,674	6.4	-0.493	Sec/SPI	0.9998	28-29	Signal Peptide	Extracellular (0.67)
lnXTH5	INIL00g00887	XM_019328024.1	I/II	scaffold0177	184,048	185,992	-	NCBI	291	3	PF00722, PF06955	32,492	5.7	-0.381	Sec/SPI	0.9997	29-30	Signal Peptide	Extracellular (0.75)
lnXTH6	INIL00g14642	XM_019333792.1	I/II	scaffold1161	313,088	314,604	-	NCBI	298	4	PF00722, PF06955	35,140	8.8	-0.566	Sec/SPI	0.9997	27-28	Signal Peptide	Extracellular (0.70)
lnXTH7	INIL02g02171	XM_019294555.1	I/II	2	33,901,936	33,903,111	+	NCBI	292	1	PF00722, PF06955	32,684	6.6	-0.395	Sec/SPI	0.9992	27-28	Signal Peptide	Extracellular (0.79)
lnXTH8	INIL02g02173	XM_019294556.1	I/II	2	33,917,163	33,918,333	-	NCBI	292	1	PF00722, PF06955	32,684	6.6	-0.395	Sec/SPI	0.9992	27-28	Signal Peptide	Extracellular (0.79)
lnXTH9	INIL02g02176	XM_019294562.1	I/II	2	33,928,615	33,929,790	+	NCBI	292	1	PF00722, PF06955	32,684	6.6	-0.395	Sec/SPI	0.9992	27-28	Signal Peptide	Extracellular (0.79)
lnXTH10	INIL03g17597	XM_019337942.1	I/II	3	32,711,764	32,713,103	-	Asagao	299	3	PF00722, PF06955	33,490	9.1	-0.432	Sec/SPI	0.9997	30-31	Signal Peptide	Extracellular (0.75)
lnXTH11	INIL03g17598	XM_019337944.1 XM_019337945.1	I/II	3	32,714,615	32,716,053	-	Asagao	299	3	PF00722, PF06955	33,467	8.6	-0.459	Sec/SPI	0.9997	30-31	Signal Peptide	Extracellular (0.75)
lnXTH12	INIL03g17599	XM_019337948.1	I/II	3	32,718,868	32,720,285	-	NCBI	289	3	PF00722, PF06955	32,460	8.5	-0.369	Sec/SPI	0.9998	23-24	Signal Peptide	Extracellular (0.86)
lnXTH13	INIL03g17601		I/II	3	32,734,342	32,735,783	-	Asagao	177	3	PF00722	19,733	5.9	-0.195	Sec/SPI	0.9996	23-24	Signal Peptide	Extracellular (0.80), Lysosome/Vacuole (0.60)
lnXTH14	INIL03g17602	XM_019337956.1	I/II	3	32,737,842	32,738,933	-	Asagao	287	2	PF00722, PF06955	32,301	8.2	-0.414	Sec/SPI	0.9998	23-24	Signal Peptide	Extracellular (0.87)
lnXTH15	INIL03g17603	XM_019337947.1	I/II	3	32,744,541	32,745,703	-	Asagao	292	2	PF00722, PF06955	32,922	7.0	-0.414	Sec/SPI	0.9998	24-25	Signal Peptide	Extracellular (0.87)
lnXTH16	INIL03g17604	XM_019337946.1	I/II	3	32,749,050	32,750,212	+	NCBI	292	2	PF00722, PF06955	32,951	8.2	-0.395	Sec/SPI	0.9998	23-24	Signal Peptide	Extracellular (0.88)
lnXTH17	INIL03g17764	XM_019338506.1	I/II	3	34,207,885	34,210,097	-	NCBI	306	4	PF00722, PF06955	35,001	6.8	-0.355	Sec/SPI	0.6206	27-28	Signal Peptide	Extracellular (0.65)
lnXTH18	INIL04g02467	XM_019299450.1	IIIA	4	12,530,243	12,532,227	-	NCBI	300	4	PF00722, PF06955	34,611	9.0	-0.474	Sec/SPI	0.9998	23-24	Signal Peptide	Endoplasmic reticulum (0.55)
lnXTH19	INIL04g28594	XM_019301646.1	I/II	4	32,446,559	32,451,843	+	Asagao	295	3	PF00722, PF06955	33,002	7.0	-0.324	Sec/SPI	0.9998	29-30	Signal Peptide	Extracellular (0.65)
lnXTH20	INIL04g34954	XM_019309641.1	I/II	4	1,564,920	1,567,128	+	Asagao	296	4	PF00722, PF06955	33,356	5.0	-0.172	Sec/SPI	0.9997	23-24	Signal Peptide	Extracellular, Lysosome/Vacuole (0.79)
lnXTH21	INIL04g34955	XM_019309987.1	I/II	4	1,567,640	1,570,350	+	Asagao	298	4	PF00722, PF06955	34,837	9.2	-0.176	Other(No SP detected)	0.5807		Signal Peptide	Extracellular (0.56)
lnXTH22	INIL05g22414	XM_019344243.1	I/II	5	29,377,303	29,379,377	-	NCBI	290	4	PF00722, PF06955	33,408	5.5	-0.410	Sec/SPI	0.9997	25-26	Signal Peptide	Extracellular (0.83)
lnXTH23	INIL07g14095	XM_019333400.1	IIIA	7	11,597,027	11,600,543	+	NCBI	314	4	PF00722, PF06955	35,524	7.2	-0.492	Sec/SPI	0.9997	39-40	Signal Peptide	Extracellular (0.57)
lnXTH24	INIL07g14097	XM_019333399.1	IIIA	7	11,655,388	11,657,487	+	NCBI	318	4	PF00722, PF06955	35,715	8.4	-0.493	Sec/SPI	0.979	43-44	Signal Peptide	Endoplasmic reticulum (0.53)
lnXTH25	INIL08g04613	XM_019321204.1	IIIB	8	4,841,872	4,844,486	-	Asagao	334	4	PF00722, PF06955	37,839	7.7	-0.416	Sec/SPI	0.9888	20-21	Signal Peptide	Extracellular (0.60)
lnXTH26	INIL08g13761	XM_019332833.1	I/II	8	10,981,180	10,983,355	+	NCBI	289	4	PF00722, PF06955	32,960	8.2	-0.444	Sec/SPI	0.9998	23-24	Signal Peptide	Extracellular (0.83)
lnXTH27	INIL09g30467	XM_019303302.1	I/II	9	3,114,472	3,116,389	-	Asagao	280	4	PF00722, PF06955	31,484	5.5	-0.367	Other(No SP detected)	1		Other	Extracellular (0.92)
lnXTH28	INIL10g12149	XM_019330706.1	IIIA	10	315,435	317,640	+	NCBI	332	4	PF00722, PF06955	37,733	9.2	-0.243	Other(No SP detected)	0.9137		Signal Peptide	Extracellular (0.53)
lnXTH29	INIL12g01243,INIL12g01244	XM_019332083.1	IIIB	12	2,736,493	2,739,321	+	NCBI	346	4	PF00722, PF06955	39,799	6.8	-0.572	Sec/SPI	0.9998	25-26	Signal Peptide	Extracellular (0.68)
lnXTH30	INIL12g22043	XM_019343467.1 XM_019343468.1	IIIA	12	59,622,390	59,624,490	-	Asagao	295	4	PF00722, PF06955	33,552	8.5	-0.560	Sec/SPI	0.9998	20-21	Signal Peptide	Extracellular (0.70)
lnXTH31	INIL13g09293	XM_019326605.1 XM_019326606.1 XM_019326607.1	I/II	13	8,743,628	8,746,101	+	Asagao	343	5	PF00722, PF06955	39,640	8.7	-0.485	Other(No SP detected)	1		Other	Endoplasmic reticulum (0.66), Golgi apparatus (0.74)
lnXTH32	INIL13g15562	XM_019335353.1	IIIB	13	12,326,135	12,330,237	-	Asagao *	319	4	PF00722, PF06955	36,768	8.8	-0.444	Sec/SPI	0.9998	22-23	Signal Peptide	Extracellular (0.65)
lnXTH33	INIL13g39072	XM_019315482.1	IIIB	13	32,800,299	32,802,344	+	Asagao	315	4	PF00722, PF06955	35,570	8.4	-0.278	Sec/SPI	0.9997	31-32	Signal Peptide	Extracellular (0.70)
lnXTH34	INIL14g03989	XM_019319025.1	I/II	14	3,944,452	3,946,439	+	Asagao	302	4	PF00722, PF06955	35,006	5.2	-0.508	Sec/SPI	0.9998	28-29	Signal Peptide	Extracellular (0.71)
lnXTH35	INIL14g42001	XM_019318842.1	I/II	14	53,250,426	53,251,878	+	Asagao	282	3	PF00722, PF06955	32,265	7.0	-0.385	Sec/SPI	0.9997	27-28	Signal Peptide	Extracellular (0.75)
lnXTH36	INIL15g28182	XM_019300959.1 XM_019300960.1	I/II	15	6,127,150	6,128,820	+	Asagao	292	4	PF00722, PF06955	33,323	8.2	-0.288	Sec/SPI	0.9996	27-28	Signal Peptide	Extracellular (0.85)

To identify relationships of the identified InXTHs, a neighbor-joining (NJ) phylogenetic tree was constructed using MEGA12 [28] (Fig. 1). A total of 36 InXTH protein sequences from morning glory, 36 IbXTH protein sequences from sweet potato [11] and 33 AtXTH protein sequences from Arabidopsis [10] were used to verify the subfamily classification. The topology of the phylogenetic tree was consistent with the established subfamily classifications from previous studies, showing no major discrepancies. Subfamily I/II was the largest group, containing 27genes. This subfamily included all four previously reported *InXTH* genes (*InXTH1–4*). The remaining were classified into Subfamily IIIA (5 genes) and Subfamily IIIB (4 genes).

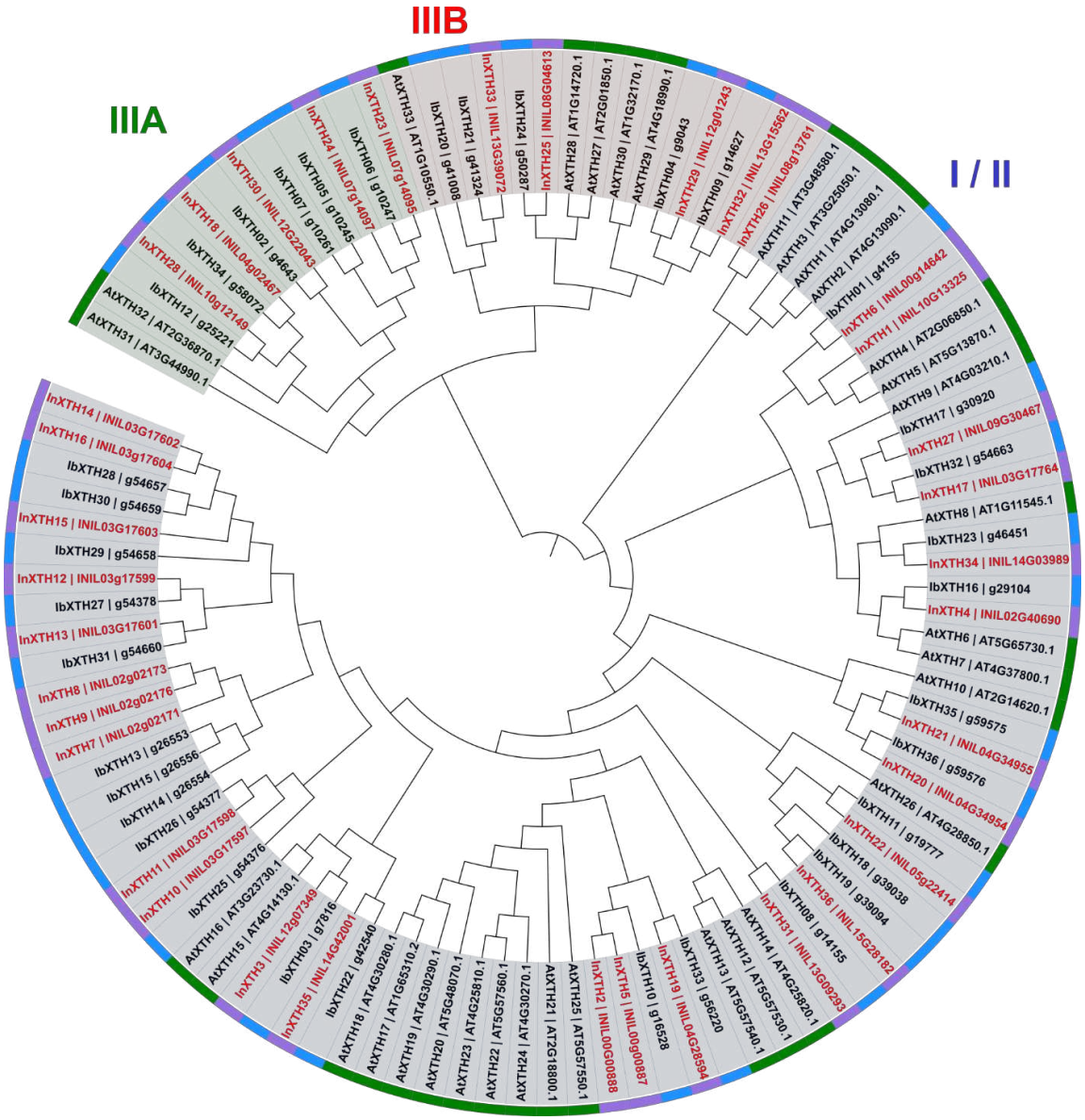

Figure1. Phylogenetic tree of the XTHs of *Ipomoea nil, I. batatas* and *Arabidopsis thaliana* . The phylogenetic tree was constructed using the Neighbor-Joining (NJ) method based on the alignment of full-length amino acid sequences of XTHs from *I. nil* (InXTHs), *I. batatas* (IbXTHs), and *A. thaliana* (AtXTHs). Color strips indicate the species of origin: purple for *I. nil*, blue for *I. batatas*, and green for *A. thaliana*. Background colors distinguish between the three major XTH subfamilies (Group I/II: light blue; Group IIIA: light green; Group IIIB: pink).

Gene structure and protein motif of InXTHs

Gene structures (exon-intron structures) of *InXTHs* were visualized by the Gene Structure Display Server 2.0 (https://gsds.gao-lab.org/) [29] based on their coding sequences (CDSs) and genomic sequences. While *InXTH* genes in Subfamily I/II contained 1 to 4 exons, all genes in Subfamily IIIA and IIIB possessed 4 exons (Fig. 2a).

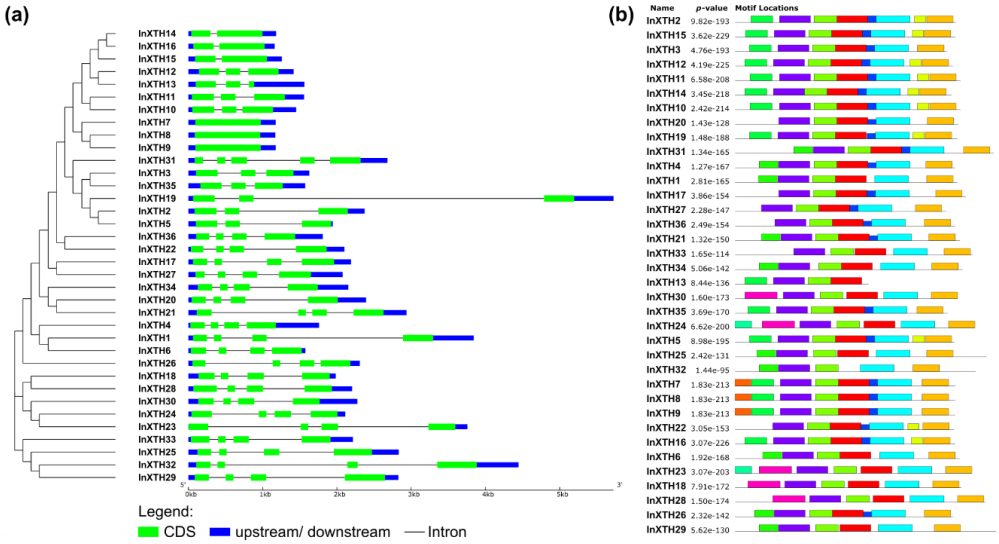

Figure 2. Gene structure and conserved protein motifs of the *InXTHs*.
(a) Exon-intron organization of *InXTH* genes. Green boxes, black lines, and blue boxes represent exons, introns, and untranslated regions (UTRs), respectively. **(b)** Distribution of conserved motifs in InXTH proteins identified by MEME analysis. Each colored box represents a distinct motif.

To characterize the InXTH proteins, conserved protein motifs were determined using MEME suite (https://meme-suite.org/meme/tools/meme) [30], and 12 conserved motifs were identified (Fig. 2b). Most of the XTHs showed highly conserved motifs in

241 the same order. Among the 12 motifs, Motif 8 was exclusively found in Subfamily IIIA
242 proteins.

243 **Chromosomal distribution and gene duplication of *InXTH*s**

244 The chromosomal distribution of 36 *InXTH* genes was visualized using MapChart
245 [31] (Fig. 3). A total of 33 *InXTH* genes were mapped onto the 15 pseudo-chromosomes,
246 while the remaining three genes (*INIL00g00887*, *INIL00g00888*, and *INIL00g14642*)
247 were located on scaffolds. The distribution of *InXTH* genes revealed an uneven
248 distribution of *InXTH* genes across the chromosomes. Chr.3 harbored the largest number
249 of *InXTHs* (8 genes), followed by Chr.2 and Chr.4 with 4 genes each. Conversely, Chr.1,
250 Chr.6, and Chr.11 did not harbor any *InXTH* gene.

251 Tandem duplications of *InXTHs* in the morning glory were estimated based on the
252 criteria established by Huang et al. (2012) [35], as two or more homologous genes within a
253 100 kbp distance. Using this criteria, five clusters of tandem duplicated *InXTHs* were
254 identified. These included a three-gene cluster on Chr.2 (*INIL02g02171*, *INIL02g02173*,
255 and *INIL02g02176*); the largest cluster comprising seven genes on Chr.3 (*INIL03g17597*,
256 *INIL03g17598*, *INIL03g17599*, *INIL03g17601*, *INIL03g17602*, *INIL03g17603*,
257 *INIL03g604*); and two-gene clusters on Chr.4 (*INIL04g34954*, *INIL04g34955*), two and

Chr.7 (*INIL07g14095*, *INIL07g14097*). Additionally, one cluster was identified on scaffold0177 (*INIL00g00887*, *INIL00g00888*).

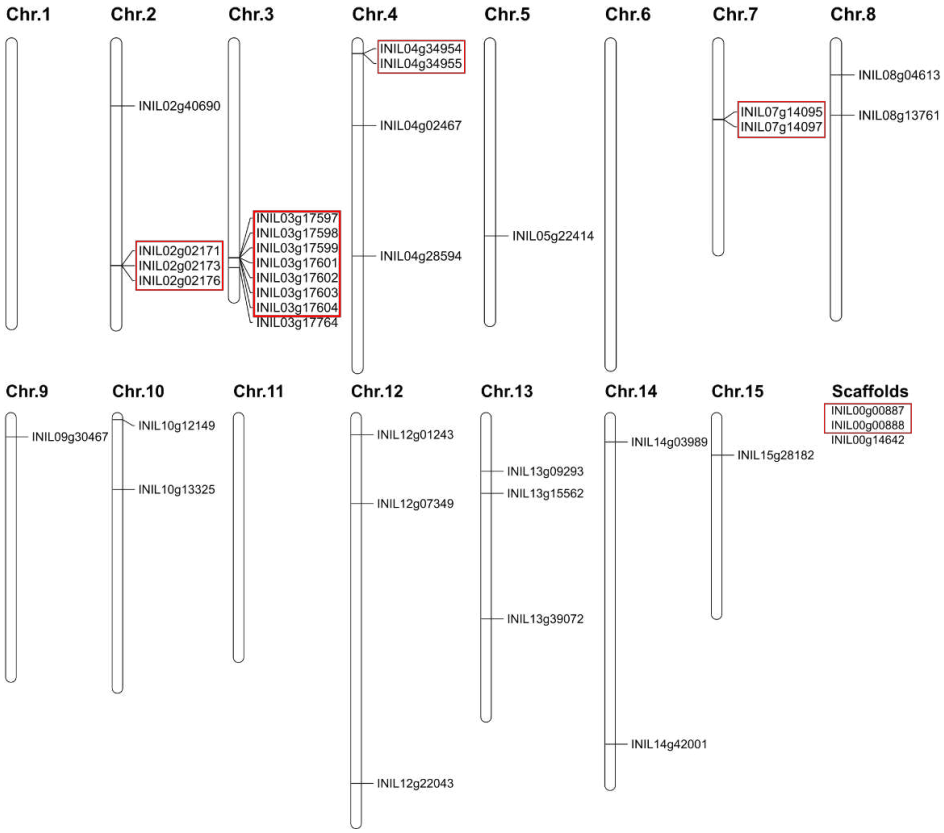

Figure 3. Chromosomal distribution of the *InXTH* genes.

The physical locations of 36 *InXTH* genes were mapped onto the 15 chromosomes and unanchored scaffolds of *I. nil* based on the Asagao Genome Database. Thirty-three genes are located on chromosomes, while three are situated on scaffolds. Red boxes indicate gene clusters resulting from duplication events. The map was generated using MapChart.

Protein property and subcellular localization of InXTHs

The physicochemical properties of the 36 identified InXTH proteins are listed in Table 1. The amino acid sequences ranged from 177 (InXTH13) to 346 (InXTH29) residues, with molecular weight (MW) spanning from 19.7 to 39.8 kDa. The theoretical

isoelectric points (pI) showed a broad distribution from 5.0 (InXTH20) to 9.3 (InXTH3), indicating diversity in the electrostatic properties of the family members. The Grand Average of Hydropathicity (GRAVY) values were consistently negative for all InXTH proteins, indicating their hydrophilic nature.

Regarding subcellular localization, SignalP 6.0 [25] predicted that 32 of the 36 InXTH proteins (88.9%) possess an N-terminal signal peptide (Sec/SPI). The prediction probabilities for the cleavage sites were high (>0.99) for the majority of these proteins. TargetP 2.0 [26] and DeepLoc 2.1 [27] classified 30 of these signal peptide-containing proteins as extracellular, consistent with the predictions from SignalP 6.0. Some proteins exhibited localization scores for the endoplasmic reticulum (ER), Golgi apparatus or vacuoles. Among the four proteins classified as lacking a signal peptide by SignalP 6.0 (InXTH21, InXTH27, InXTH28, and InXTH31), two (InXTH21 and InXTH28) were predicted to possess a signal peptide by TargetP 2.0 and were classified as extracellular by DeepLoc 2.1. The remaining two InXTHs (InXTH27 and InXTH31) consistently lacked signal peptide predictions across multiple tools.

Gene expression profile of *InXTHs* in different organs

To elucidate the organ-specific expression patterns of *InXTH* genes, we analyzed RNA-seq data covering six organs (root, stem, leaf, flower, seed coat, and embryo) obtained from the Asagao1.2 database. The gene expression profiles of all 36 *InXTHs* were visualized in a heatmap (Fig. 4). A gene was considered expressed if its RPKM value exceeded 0.5, a threshold consistent with the preprocessing parameters used for the subsequent WGCNA. The total expression levels of *InXTH* genes varied among organs. The highest total RPKM was observed in stems and roots, followed by flowers and seed coats, with the lowest expression levels in leaves and embryos. Expression levels also varied by subfamily classification. Genes in Subfamily I/II generally exhibited expression across multiple organs. In contrast, Subfamilies IIIA and IIIB showed specific expressions among the organs. Within Subfamily IIIA, only three genes (*InXTH23*, *InXTH28*, and *InXTH30*) showed detectable expression. Similarly, in Subfamily IIIB, only *InXTH25* exceeded the detection threshold.

Based on the RPKM threshold (> 0.5), seven genes (*InXTH1*, *InXTH3*, *InXTH10*, *InXTH16*, *InXTH17*, *InXTH27,* and *InXTH34*) were identified as constitutively expressed across all analyzed organs. The previously reported genes *InXTH1–4* exhibited high expression not only in flowers but also in stems and roots, implying that they play a

304 constitutive role in cell expansion throughout plant development. Conversely, five genes
305 (*InXTH5*, *InXTH6*, *InXTH18*, *InXTH24,* and *InXTH31*) exhibited RPKM values below
306 0.5 in all organs, suggesting potential pseudogenization or specific expression under
307 specific conditions.

308 Regarding organ specificity, distinct expression patterns were observed in flowers
309 and the seed coat. Three tandemly duplicated genes (*InXTH7*, *InXTH8*, and *InXTH9*)
310 exhibited flower specific expression. These genes showed high expression (RPKM > 150)
311 in flowers, while their expression levels remained below the threshold (RPKM < 0.5) in
312 other organs. Additionally, *InXTH20* exhibited specific expression in the seed coat,
313 accounting for approximately half of the total *XTH* expression in this organ.

314 Furthermore, we examined the expression divergence within tandemly duplicated
315 gene clusters identified in the chromosomal analysis. A marked expression divergence
316 was observed in the *InXTH2*, *InXTH5* tandem pair. While *InXTH2* was highly expressed
317 especially in roots, its paralog *InXTH5* showed no expression across all organs. A contrast
318 in expression profiles was also found in the putative tandem pair *InXTH20* and *InXTH21*.
319 While *InXTH20* was predominantly expressed in the seed coat, its paralog *InXTH21*
320 exhibited only weak expression in roots, stems, and flowers, suggesting functional
321 differentiation. In the *InXTH10–InXTH16* cluster, *InXTH10* and *InXTH16* showed

constitutive expression, whereas other members showed restricted expression. Collectively, these contrasting expression profiles suggest that tandemly duplicated *InXTH* genes have acquired distinct transcriptional regulation, leading to their functional divergence following duplication events.

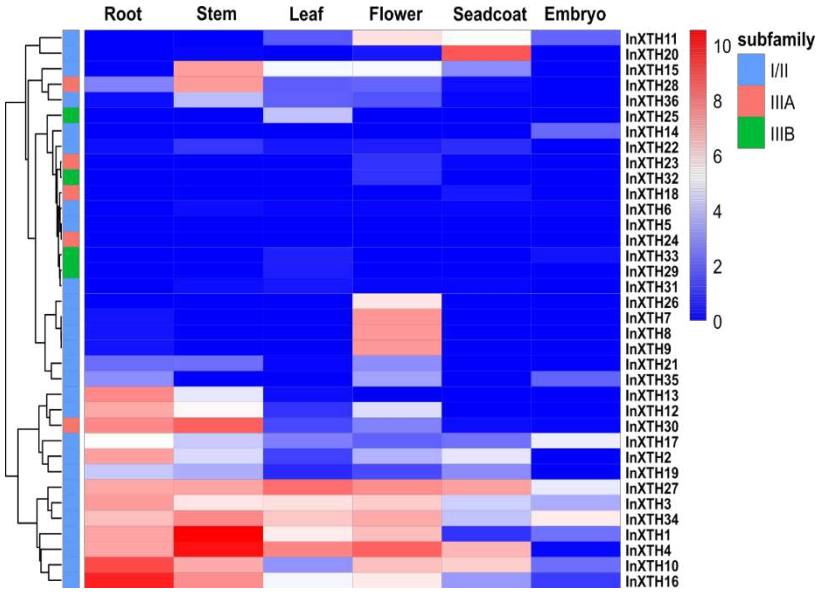

Figure 4. Tissue-specific gene expression profiles of the *InXTHs*.
Heatmap visualization of *InXTH* gene expression across various organs based on RNA-seq data from the Asagao Genome Database. Gene expression levels are presented as log2-transformed RPKM values [log2(RPKM +1)]. Genes (rows) are clustered hierarchically based on expression similarity, while tissues (columns) are arranged in anatomical order. The color scale ranges from blue (low expression) to red (high expression). Note that for *InXTH29*, which is annotated as two separate fragments in the database, RPKM values represent the length-weighted average of the fragments to correct for this annotation error.

Gene expression profile of *InXTHs* during petal development and senescence

To elucidate functions of InXTHs in petal, including development of petal, flower opening and closing, the temporal gene expressions of *InXTHs* in petal was profiled

339 utilizing the time-course transcriptome database for Japanese morning glory petals by
340 Nakagawa et al. [21] (Fig. 5). Within Subfamily I/II members, *InXTH4* exhibited the highest
341 expression among all *InXTH* genes, with a maximum FPKM value exceeding 18,000 (Fig.
342 5a). Transcript levels increased during the dark period prior to anthesis and reached a
343 peak at the time of flower opening (0 h). *InXTH1* also showed high expression (maximum
344 FPKM > 7,000) but displayed a different temporal pattern, peaking 3 h before flower
345 opening. While other Subfamily I/II members were detected, their expression levels were
346 substantially lower compared to the dominant *InXTH4* and *InXTH1*.

347 Genes in Subfamily IIIA generally showed low expression throughout the examined
348 period (Fig. 5b). Specific temporal patterns were detected, such as a gradual decrease in
349 *InXTH28* from 72 h before flower opening and a minor peak in *InXTH30* at 6 h post-
350 flowering. However, their absolute expression levels remained low. In contrast, within
351 Subfamily IIIB, only *InXTH29* exhibited a distinct expression peak (Fig. 5c). It reached
352 a maximum FPKM exceeding 600 at 6 h before flower opening, whereas other genes
353 remained at negligible levels.

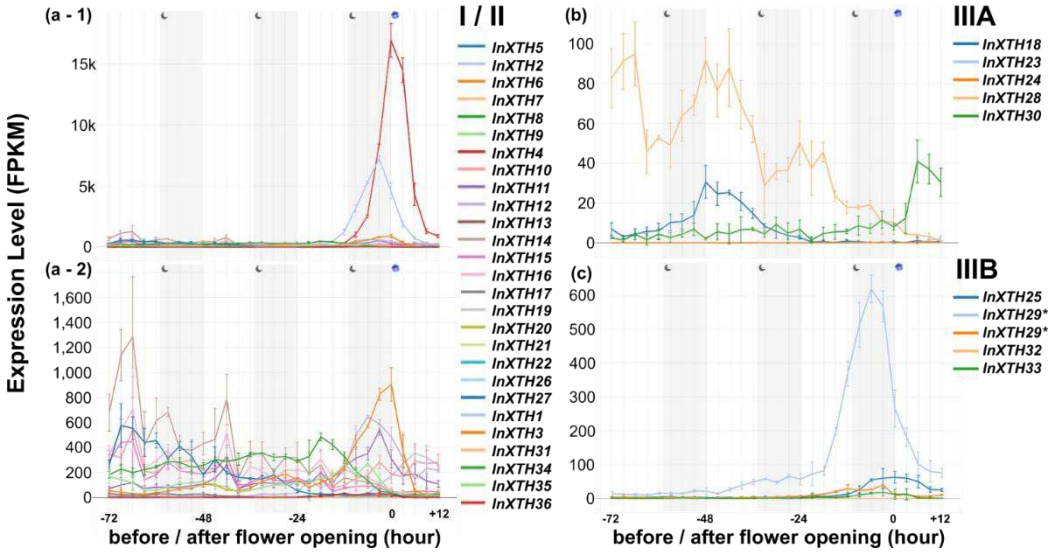

Figure 5. Gene expression profiles of the *InXTHs* in the petals before and after flower opening.

Gene expression patterns of the *InXTH*s were obtained from the temporal transcriptome data and interactive database (https://ipomoeanil.nibb.ac.jp/fpkm/). The plots display the expression levels (FPKM) from 3-h interval from 72 h before and 12 h after flower opening. (a-1) Full scale plots of Group I/II subfamily. (a-2) A magnified view of (a-1) focusing on genes with lower expression levels. (b) Group IIIA subfamily. (c) Group IIIB subfamily. Each line corresponds to an individual *InXTH* gene. Note that *InXTH29* is represented by two separate lines due to split gene annotation in the database.

Weighted gene co-expression network analysis (WGCNA)

To elucidate the gene regulatory networks associated with *InXTHs,* we performed a WGCNA using the time-course transcriptome data. To ensure the robustness of the network, we first optimized the number of genes included in the analysis by evaluating the scale-free topology fit index (R^2) across datasets with varying numbers of high-CV (coefficient of variation) genes. The subset of the top 7,000 variable genes yielded the optimal scale-free topology using a soft-thresholding power of β=5. By combining these

high-CV genes with 32 *InXTH* genes that showed detectable expression (FPKM > 0.5), a total of 7,023 genes were subjected to the analysis. Hierarchical clustering based on topological overlap identified 24 distinct co-expression modules, which varied widely in size from 49 to 2,838 genes (Supplemental Fig. S1). To assess the reliability of module assignments for *InXTH* genes, module membership (kME) was calculated for each gene as the correlation with its assigned module eigengene. Nine *InXTH* genes with kME < 0.3 were excluded from subsequent module-based analyses, as they did not exhibit reliable co-expression patterns. The 23 *InXTH* genes were distributed across six modules: turquoise (n = 6), blue (n = 3), brown (n = 1), yellow (n = 2), red (n = 10), and grey (n = 1). The grey module comprises genes that could not be assigned to any specific co-expression cluster.

Analysis of module eigengenes revealed distinct temporal trends across the identified modules (Fig. 6). The blue module exhibited a gradual decrease in expression starting approximately 69 h before flower opening. Transitioning toward anthesis, the red module showed a peak between 6 and 3 h before flower opening, followed by the yellow module, which peaked at the time of flower opening (0 h). In the post- flower opening phase, the brown module exhibited a peak at 3 h, whereas the turquoise module showed a continuous increasing trend after the brown module.

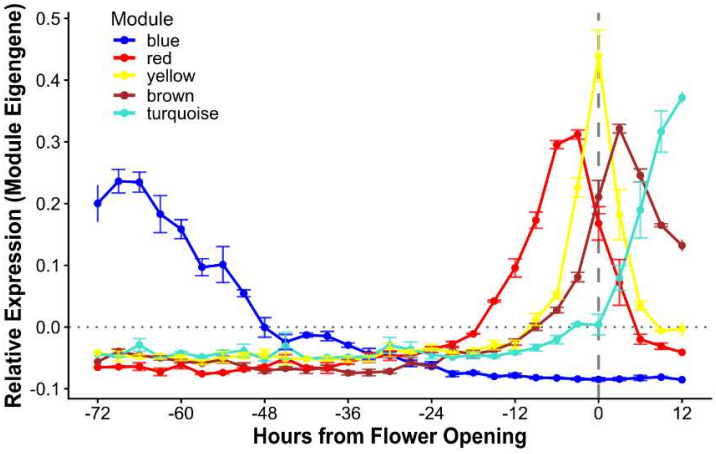

Figure 6. Temporal gene expression profiles of co-expression modules identified by WGCNA. Profiles of module eigengenes for the five selected modules (blue, red, yellow, brown, and turquoise) during petal development. The x-axis represents the time in hours relative to flower opening (0 h; indicated by the vertical dashed line). The y-axis represents the module eigengene value, indicating the relative expression pattern of each module. Data points and lines indicate the mean values, and error bars represent the standard error (SE) of biological replicates (n = 3).

Functional characterization of *InXTH* co-expression modules

To clarify the biological functions of each module in WGCNA, we next analyzed the expression profiles and intramodular connectivity (k_{ME}) of the constituent genes. Figure 7 summarizes the maximum expression levels of the *InXTH* genes assigned to the five key modules (blue, red, yellow, brown, and turquoise). Based on these profiles, we identified hub genes characterized by high connectivity ($k_{ME} > 0.8$) and expression levels (Supplemental Table S3). Additionally, Gene Ontology (GO) enrichment analysis was performed to characterize the biological processes associated with each module (Supplemental Fig. S2).

The blue module exhibited a distinct temporal profile, peaking at 69 to 66 h before flower opening, decreasing to 48 h, and maintaining a low basal level thereafter. Consistent with this trend, the module was significantly enriched in GO terms related to "cell division" and "cell cycle." Notably, *InXTH27* (k_{ME} = 0.80) was identified as a highly expressed hub gene within this cluster. This downregulation pattern matches the cessation of cell division activity at approximately 48 h before anthesis as reported previously [21]. Consequently, *InXTH27* expression is temporally correlated with the cell proliferation phase.

The red module (peaking 3–6 h before anthesis) and the yellow module (peaking at 0 h) exhibited contrasting expression patterns regarding *XTH* genes. The red module was characterized by the coordinated expression of multiple *InXTH* genes. *InXTH1* was identified as a highly expressed hub gene (k_{ME} = 0.93), co-expressed with *InXTH12*, *InXTH29*, *InXTH33*, and *InXTH36*, along with cell wall-modifying enzymes such as pectinesterase. This indicates that a specific subset of XTH isozymes and cell wall enzymes are transcriptionally co-regulated prior to flower opening.

In contrast, the yellow module was predominantly driven by a single *XTH* gene, *InXTH4*. *InXTH4* showed the highest expression level among the *InXTH* family members (Max FPKM > 18,000) and appeared as a dominant hub (k_{ME} = 0.84), co-expressed with

auxin-responsive genes like *SAUR72* and *SAUR50-like*. This implies that the rapid petal expansion at anthesis is not orchestrated by a diverse set of *XTHs*, but rather by the robust induction of *InXTH4*.

The brown module, which peaked 3 h after flower opening, contained putative epigenetic regulators, including *histone H2A* and *methyl-CpG-binding domain-containing protein 6*. The presence of these factors indicates that the expression of chromatin remodeling components temporally coincides with the transition from open flower to the onset of senescence. In the brown module, *InXTH2* (k_{ME} = 0.90) was identified as a highly expressed hub gene.

The turquoise module, showing an increasing trend after flower opening, contained genes associated with protein degradation and transcriptional regulation, such as *SKP1-like proteins* and *WRKY transcription factor 75*. Six *InXTH* genes were assigned to this module and co-expressed with these senescence-associated hubs. The expression pattern is consistent with the progression of petal wilting, implicating a subset of InXTHs in the senescence process.

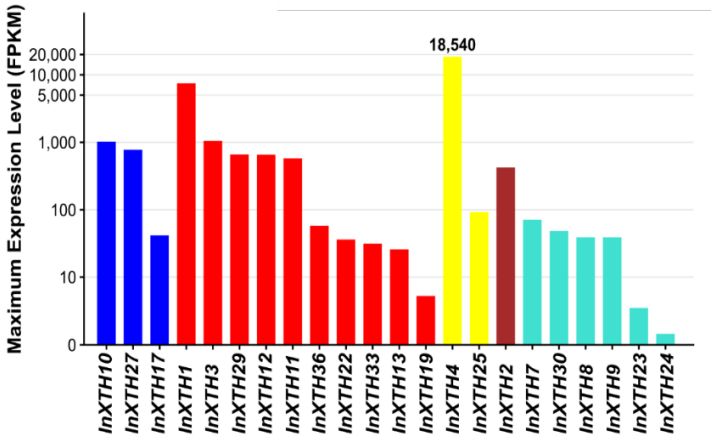

Figure 7. Maximum expression levels of *InXTH* genes across co-expression modules. The bar chart displays the maximum expression level (FPKM) recorded for each *InXTH* gene across the entire developmental time course. Genes are grouped by their assigned WGCNA modules (blue, red, yellow, brown, and turquoise) and sorted within each module in descending order. The y-axis is presented on a pseudo-logarithmic. Bar colors correspond to the module colors. Numerical labels indicate the exact FPKM values for genes showing exceptionally high expression (>10,000 FPKM).

4. Discussion

The identification of 36 *InXTH* genes in the *I. nil* genome highlighted an expansion of the *XTH* gene family in the *I. nil* compared to other plants (Fig. 1). The subfamily distribution in I. nil (Group I/II: 27, IIIA: 5, IIIB: 4) is largely comparable to that of its close relative, *I. batatas* (Group I/II: 25, IIIA: 6, IIIB: 5) [11]. However, the slight increase in Group I/II members in I. nil suggests that lineage-specific gene duplications have occurred after the divergence of these two species, contributing to the distinct evolutionary path of the *I. nil* genome.

458 Chromosomal distribution analysis revealed that *InXTH* genes are unevenly
459 distributed, forming five distinct clusters (Fig. 3). Notably, the largest cluster on Chr.3
460 contains seven *XTH* genes within a narrow physical distance. This genomic organization
461 mirrors the arrangement observed in *I. batatas*, where a major *XTH* cluster is located on
462 Chr.13 [11], suggesting that these clusters originated from a common ancestor prior to
463 speciation. Interestingly, phylogenetic analysis revealed a complex evolutionary history
464 for these clustered genes, in which some *InXTH* members formed orthologous pairs with
465 *IbXTHs*, whereas others formed paralogous clades solely within *I. nil*. This pattern
466 suggests that the expansion of the *InXTH* family resulted from a combination of ancient
467 segmental duplications shared by the genus *Ipomoea* and recent, lineage-specific tandem
468 duplications specific to *I. nil*. Consequently, the gene cluster on Chr.3 appears to be a
469 major site of such duplication events, which likely contributed to the functional
470 diversification of the family.

471 XTH enzymes function in the apoplast for cell wall remodeling [5]. Secretion of these
472 proteins to the apoplast typically requires an N-terminal signal peptide [36]. Consistent with
473 this expectation, our analysis showed that most InXTHs (88.9%) contained a predicted
474 signal peptide and are classified as extracellular, supporting their expected roles in cell
475 expansion (Table. 1). However, a few InXTHs showed atypical localization predictions.

476 Predicted localization to the ER or Golgi apparatus may reflect transient residence within
477 the conventional secretory pathway. The absence of a predicted signal peptide in
478 InXTH27 and InXTH31 may have resulted from misannotation of the start codon, or
479 potentially atypical secretion mechanisms. Although most cell wall proteins are secreted
480 via the conventional signal peptide–dependent pathway, non-canonical cell wall proteins
481 lacking signal peptides have occasionally been reported [36]. However, such proteins are
482 often considered potential contaminants in cell wall proteomic analyses, and their
483 extracellular localization requires careful validation.

484 Regarding transcriptional regulation, our comprehensive profiling (Fig. 4 and 5)
485 revealed that *InXTH* expression patterns are not strictly correlated with their phylogenetic
486 classification (Fig. 1). Genes belonging to different subfamilies exhibited expression
487 peaks mostly around anthesis and during senescence. This observation suggests that the
488 transcriptional regulation of *XTH* genes has evolved independently of their coding
489 sequences. Rather than being constrained by subfamily identity, distinct *XTH* genes
490 appear to have been recruited to function at specific developmental stages, such as flower
491 opening and senescence. This divergence in expression patterns is indicative of
492 subfunctionalization, allowing distinct isozymes to specialize in specific developmental
493 phases. Consequently, distinct *XTH* isozymes appear to be deployed at different

494 developmental phases, likely contributing to the precise cell wall remodeling required for
495 petal morphogenesis.

496 This study revealed that the expression of *InXTH* genes is not uniform throughout
497 petal development but is orchestrated in a distinct, stage-specific manner (Fig. 6). Among
498 the co-expression modules identified by WGCNA, we focused on five *InXTH*-containing
499 modules that correspond to specific developmental phases, including cell proliferation in
500 the blue module, preparation for anthesis in the red module, rapid expansion in the yellow
501 module, and the transition to senescence in the brown and turquoise modules
502 (Supplemental Fig. S2). These findings suggest that distinct XTH isozymes are recruited
503 to fulfill specific cell wall remodeling requirements at each developmental stage, rather
504 than being mediated by a single enzyme handling the entire process.

505 The blue module, represented by *InXTH27*, exhibited preferential transcript
506 accumulation until 48 h before flower opening (Fig. 6). This period coincides with the
507 active cell division phase in *I. nil* petals [21]. While XTH family enzymes are most widely
508 documented for their roles in facilitating cell wall loosening during rapid cell expansion
509 [34], the specific temporal correlation of *InXTH27* with the proliferation phase implies a
510 distinct physiological function. This isozyme likely contributes to the cell wall
511 remodeling required for cytokinesis or the post-mitotic enlargement of daughter cells [37] .

512 Given that the primary cell wall must be dynamic to accommodate cell plate formation
513 [4,38], *InXTH27* may facilitate the structural modification of the nascent wall network. This
514 hypothesis is supported by a recent finding that specific Arabidopsis *XTH* members,
515 *AtXTH4* and *AtXTH7*, are essential for callus proliferation during graft union formation
516 [39]. Phylogenetically, *InXTH17* and *InXTH27* belong to the broader clade which includes
517 these proliferation-associated *AtXTHs*. Coupled with their transcript accumulation during
518 the early development stages, this phylogenetic similarity implies that these blue module
519 *InXTHs* possibly share a conserved function regarding cell wall plasticity for active cell
520 division.

521 Immediately prior to flower opening (-6 to -3 h), the red module was characterized
522 by the concurrent upregulation of multiple *InXTH* genes alongside a cell wall-modifying
523 enzyme (*pectinesterase*) and a *potassium transporter* (Supplemental Table S3 and Fig. 6).
524 Specifically, the presence of *InXTH1* in this pre-opening phase is consistent with previous
525 findings that *InXTH1* expression is closely correlated with petal elongation [33].The co-
526 expression of different *XTH* subfamilies implies that isozymes with distinct enzymatic
527 properties may act in a complementary manner to facilitate effective cell wall loosening
528 and remodeling [34]. Furthermore, the presence of *pectinesterase* suggests that modification
529 of the pectin matrix occurs in parallel with xyloglucan remodeling, likely to modulate the

530 cell wall mechanical properties for the impending expansion [40]. In addition, the
531 upregulation of the *potassium transporter* indicates that solute accumulation begins prior
532 to full opening, priming the cells for the turgor-driven expansion that follows[41].

533 The yellow module, peaking at the time of flower opening, was dominated by the
534 robust expression of *InXTH4* (Fig.6, 7). Considering the ephemeral nature of the one-day
535 flower of *I. nil*, in which full opening occurs rapidly within a limited time [21], these results
536 suggest that *InXTH4* acts as a principal driver of this rapid petal unfolding. This result is
537 consistent with the previous study by Shinozaki et al. (2014), which identified *InXTH4* as
538 a key gene whose expression dictates the rate of flower opening under different
539 photoperiods [33]. Notably, this module also contained two co-expressed SAUR (small
540 auxin upregulated RNA) genes (Supplemental Table S3). SAUR proteins are established
541 effectors of the acid growth mechanism, promoting cell elongation through the activation
542 of H^+-ATPases and consequent apoplastic acidification [42]. The synchronized gene
543 expression of *InXTH4* and *SAUR* supports the hypothesis that auxin-mediated apoplastic
544 acidification could create a favorable environment for *InXTH4* activity [8], thereby
545 facilitating the substantial cell expansion observed at anthesis.

546 Following anthesis, the brown module, which peaked at 3 h after flower opening,
547 showed the upregulation of several putative epigenetic regulators, including genes

548 annotated as *histone H2A* and *methyl-CpG-binding domain proteins* (Supplemental Table
549 S3and Fig. 6). This timing coincides with the transition from the fully open state to the
550 onset of petal wilting. The induction of these chromatin-associated factors suggests that
551 transcriptional reprogramming may occur at this stage, potentially contributing to the
552 repression of growth-associated genes and the initiation of senescence-related pathways
553 [43].

554 Subsequently, the turquoise module, which increased during wilting, was enriched
555 in hubs associated with protein degradation, e.g., *SKP1-like proteins*, and transcriptional
556 regulation (Supplemental Table S3 and Fig. 6). A prominent hub was *WRKY75*, a
557 transcription factor known to act as a positive regulator of senescence in Arabidopsis [44].
558 The co-expression of specific *InXTH* genes within this module suggests that cell wall
559 modification or disassembly accompanies the senescence program, possibly facilitating
560 nutrient remobilization from degenerating petal organs to plant body. Therefore, the
561 expression profile of this module is consistent with transcriptomic evidence showing that
562 autophagy-related and transporter genes are coordinately upregulated during petal
563 senescence, supporting nutrient remobilization [21].

564 Collectively, the time-resolved co-expression analysis reveals a sequential
565 transcriptional program in which distinct XTH isozymes are engaged at successive stages

of petal development, coupling cell wall remodeling to cell proliferation, rapid expansion at anthesis, and ordered disassembly during senescence.

References

1 van Doorn, W. & van Meeteren, U. Flower opening and closure: a review. *JOURNAL OF EXPERIMENTAL BOTANY* **54**, 1801-1812 (2003). https://doi.org/10.1093/jxb/erg213

2 Yamada, K., Norikoshi, R., Suzuki, K., Imanishi, H. & Ichimura, K. Determination of subcellular concentrations of soluble carbohydrates in rose petals during opening by nonaqueous fractionation method combined with infiltration-centrifugation method. *PLANTA* **230**, 1115-1127 (2009). https://doi.org/10.1007/s00425-009-1011-6

3 Cosgrove, D. Growth of the plant cell wall. *NATURE REVIEWS MOLECULAR CELL BIOLOGY* **6**, 850-861 (2005). https://doi.org/10.1038/nrm1746

4 Fry, S. Primary cell wall metabolism: tracking the careers of wall polymers in living plant cells. *NEW PHYTOLOGIST* **161**, 641-675 (2004). https://doi.org/10.1111/j.1469-8137.2004.00980.x

5 Rose, J., Braam, J., Fry, S. & Nishitani, K. The XTH family of enzymes involved in xyloglucan endotransglucosylation and endohydrolysis: current perspectives and a new unifying nomenclature. *PLANT AND CELL PHYSIOLOGY* **43**, 1421-1435 (2002). https://doi.org/10.1093/pcp/pcf171

6 Nishitani, K. & Tominaga, R. Endoxyloglucan transferase, a novel class of glycosyltransferase that catalyzes transfer of a segment of xyloglucan molecule to another xyloglucan molecule. *JOURNAL OF BIOLOGICAL CHEMISTRY* **267**, 21058-21064 (1992).

7 Desilva, J. *et al.* Molecular characterization of a xyloglucan-specific endo-(1-]4)-beta-D-glucanase (xyloglucan endotransglycosylase) from nasturtium seeds. *PLANT JOURNAL* **3**, 701-711 (1993).

8 Maris, A. *et al.* Differences in enzymic properties of five recombinant xyloglucan endotransglucosylase/hydrolase (XTH) proteins of Arabidopsis thaliana. *JOURNAL OF EXPERIMENTAL BOTANY* **62**, 261-271 (2011). https://doi.org/10.1093/jxb/erq263

9 Yokoyama, R. & Nishitani, K. A comprehensive expression analysis of all members of a gene family encoding cell-wall enzymes allowed us to predict cis-regulatory regions involved in cell-wall construction in specific organs of arabidopsis. *PLANT AND CELL PHYSIOLOGY* **42**, 1025-1033 (2001). https://doi.org/10.1093/pcp/pce154

10 Yokoyama, R., Rose, J. & Nishitani, K. A surprising diversity and abundance of xyloglucan endotransglucosylase/hydrolases in rice. Classification and expression analysis. *PLANT PHYSIOLOGY* **134**, 1088-1099 (2004). https://doi.org/10.1104/pp.103.035261

11 Zhang, J. *et al.* Genome-wide identification and expression analysis of the xyloglucan endotransglucosylase/hydrolase gene family in sweet potato [Ipomoea batatas (L.) Lam]. *INTERNATIONAL JOURNAL OF MOLECULAR SCIENCES* **24** (2023). https://doi.org/10.3390/ijms24010775

12 Osato, Y., Yokoyama, R. & Nishitani, K. A principal role for AtXTH18 in Arabidopsis thaliana root growth: a functional analysis using RNAi plants. *JOURNAL OF PLANT RESEARCH* **119**, 153-162 (2006). https://doi.org/10.1007/s10265-006-0262-6

13 Vissenberg, K., Fry, S. & Verbelen, J. Root hair initiation is coupled to a highly localized increase of xyloglucan endotransglycosylase action in arabidopsis roots. *PLANT PHYSIOLOGY* **127**, 1125-1135 (2001). https://doi.org/10.1104/pp.127.3.1125

14 Han, Y. *et al.* Isolation and characterization of two persimmon xyloglucan endotransglycosylase/hydrolase (XTH) genes that have divergent functions in cell wall modification and fruit postharvest softening. *FRONTIERS IN PLANT SCIENCE* **7** (2016). https://doi.org/10.3389/fpls.2016.00624

15 Harada, T. *et al.* Cloning, characterization, and expression of xyloglucan endotransglucosylase/hydrolase and expansin genes associated with petal growth and development during carnation flower opening. *JOURNAL OF EXPERIMENTAL BOTANY* **62**, 815-823 (2011). https://doi.org/10.1093/jxb/erq319

16 Yang, Y. *et al.* Genome-wide identification and expression analysis of XTH gene family during flower-opening stages in Osmanthus fragrans. *PLANTS-BASEL* **11** (2022). https://doi.org/10.3390/plants11081015

17 Hayama, R., Agashe, B., Luley, E., King, R. & Coupland, G. A circadian rhythm set by dusk determines the expression of FT homologs and the short-day photoperiodic flowering response in Pharbitis. *PLANT CELL* **19**, 2988-3000 (2007). https://doi.org/10.1105/tpc.107.052480

18 Morita, Y. & Hoshino, A. Recent advances in flower color variation and patterning of Japanese morning glory and petunia. *BREEDING SCIENCE* **68**, 128-138 (2018). https://doi.org/10.1270/jsbbs.17107

19 Shibuya, K., Shimizu, K., Niki, T. & Ichimura, K. Identification of a NAC transcription factor, EPHEMERAL1, that controls petal senescence in Japanese morning glory. *PLANT JOURNAL* **79**, 1044-1051 (2014). https://doi.org/10.1111/tpj.12605

20 Hoshino, A. *et al.* Genome sequence and analysis of the Japanese morning glory Ipomoea nil. *Nature Communications* **7**, 13295 (2016). https://doi.org/10.1038/ncomms13295

21 Nakagawa, S. *et al.* Transcriptomic dynamics of petal development in the one-day flower species, Japanese morning glory (Ipomoea nil). *PLANT AND CELL PHYSIOLOGY* **66**, 1823-1838 (2025). https://doi.org/10.1093/pcp/pcaf108

22 Berardini, T. *et al.* The arabidopsis information resource: Making and mining the "gold standard" annotated reference plant genome. *GENESIS* **53**, 474-485 (2015). https://doi.org/10.1002/dvg.22877

23 Paysan-Lafosse, T. *et al.* InterPro in 2022. *NUCLEIC ACIDS RESEARCH* **51**, D418-D427 (2023). https://doi.org/10.1093/nar/gkac993

24 Mistry, J. *et al.* Pfam: The protein families database in 2021. *NUCLEIC ACIDS RESEARCH* **49**, D412-D419 (2021). https://doi.org/10.1093/nar/gkaa913

25 Teufel, F. *et al.* SignalP 6.0 predicts all five types of signal peptides using protein language models. *NATURE BIOTECHNOLOGY* **40**, 1023-+ (2022). https://doi.org/10.1038/s41587-021-01156-3

26 Armenteros, J. *et al.* Detecting sequence signals in targeting peptides using deep learning. *LIFE SCIENCE ALLIANCE* **2** (2019). https://doi.org/10.26508/lsa.201900429

27 Odum, M. *et al.* DeepLoc 2.1: multi-label membrane protein type prediction using protein language models. *NUCLEIC ACIDS RESEARCH* **52**, W215-W220 (2024). https://doi.org/10.1093/nar/gkae237

28 Kumar, S. *et al.* MEGA12: Molecular evolutionary genetic analysis version 12 for adaptive and green computing. *MOLECULAR BIOLOGY AND EVOLUTION* **41** (2024). https://doi.org/10.1093/molbev/msae263

29 Hu, B. *et al.* GSDS 2.0: an upgraded gene feature visualization server. *BIOINFORMATICS* **31**, 1296-1297 (2015). https://doi.org/10.1093/bioinformatics/btu817

30 Bailey, T., Johnson, J., Grant, C. & Noble, W. The MEME Suite. *NUCLEIC ACIDS RESEARCH* **43**, W39-W49 (2015). https://doi.org/10.1093/nar/gkv416

31 Voorrips, R. MapChart: Software for the graphical presentation of linkage maps and QTLs. *JOURNAL OF HEREDITY* **93**, 77-78 (2002). https://doi.org/10.1093/jhered/93.1.77

32 Langfelder, P. & Horvath, S. WGCNA: an R package for weighted correlation network analysis. *BMC BIOINFORMATICS* **9** (2008). https://doi.org/10.1186/1471-2105-9-559

33 Shinozaki, Y. *et al.* Length of the dark period affects flower opening and the expression of circadian-clock associated genes as well as xyloglucan endotransglucosylase/hydrolase genes in petals of morning glory (Ipomoea nil). *PLANT CELL REPORTS* **33**, 1121-1131 (2014). https://doi.org/10.1007/s00299-014-1601-z

34 Eklof, J. & Brumer, H. The XTH gene family: an update on enzyme structure, function, and phylogeny in xyloglucan remodeling. *PLANT PHYSIOLOGY* **153**, 456-466 (2010). https://doi.org/10.1104/pp.110.156844

35 Huang, S. *et al.* Genome-wide analysis of WRKY transcription factors in Solanum lycopersicum. *MOLECULAR GENETICS AND GENOMICS* **287**, 495-513 (2012). https://doi.org/10.1007/s00438-012-0696-6

36 Jamet, E., Canut, H., Boudart, G. & Pont-Lezica, R. Cell wall proteins: a new insight through proteomics. *TRENDS IN PLANT SCIENCE* **11**, 33-39 (2006). https://doi.org/10.1016/j.tplants.2005.11.006

37 Matsui, A. *et al.* AtXTH27 plays an essential role in cell wall modification during the development of tracheary elements. *PLANT JOURNAL* **42**, 525-534 (2005). https://doi.org/10.1111/j.1365-313X.2005.02395.x

38 Jürgens, G. Cytokinesis in higher plants. *ANNUAL REVIEW OF PLANT BIOLOGY* **56**, 281-299 (2005). https://doi.org/10.1146/annurev.arplant.55.031903.141636

39 Xiong, M. *et al.* Xyloglucan endotransglucosylase/hydrolase family genes are required for the plant graft union formation through callus proliferation. *PLANT PHYSIOLOGY* **200** (2026). https://doi.org/10.1093/plphys/kiag030

40 Wolf, S. & Greiner, S. Growth control by cell wall pectins. *PROTOPLASMA* **249**, 169-175 (2012). https://doi.org/10.1007/s00709-011-0371-5

41 Shabala, S. & Lew, R. Turgor regulation in osmotically stressed Arabidopsis epidermal root cells. Direct support for the role of inorganic ion uptake as revealed by concurrent flux and cell turgor measurements. *PLANT PHYSIOLOGY* **129**, 290-299 (2002). https://doi.org/10.1104/pp.020005

42 Spartz, A. *et al.* SAUR inhibition of PP2C-D phosphatases activates plasma membrane H+-ATPases to promote cell expansion in Arabidopsis. *PLANT CELL* **26**, 2129-2142 (2014). https://doi.org/10.1105/tpc.114.126037

43 Feng, S. *et al.* DNA methylation remodeled amino acids biosynthesis regulates flower senescence in carnation (Dianthus caryophyllus). *NEW PHYTOLOGIST* **241**, 1605-1620 (2024). https://doi.org/10.1111/nph.19499

44 Guo, P. *et al.* A tripartite amplification loop involving the transcription factor WRKY75, salicylic acid, and reactive oxygen species accelerates leaf senescence. *PLANT CELL* **29**, 2854-2870 (2017). https://doi.org/10.1105/tpc.17.00438

Acknowledgements

This work was supported by JSPS KAKENHI Grant Numbers 24K01745 and 21H02184.

Funding

This work was supported by JSPS KAKENHI Grant Numbers 24K01745 and 21H02184.

Data Availability

The genomic data analyzed in this study are publicly available in the Japanese morning glory genome database (Asagao1.2 database, http://viewer.shigen.info/asagao/) and NCBI database under accession number BDFN00000000.1. The datasets generated during the analysis are available from the corresponding author on reasonable request.

Contributions

K.Y. and K.S. conceived the study and designed the study. K.Y. performed the bioinformatic analyses and wrote the manuscript. K.S. reviewed and edited the manuscript and supervised the project. All authors reviewed and approved the final manuscript.

Corresponding author

Correspondence to Katsuhiro Shiratake.

Competing interests

The authors declare no competing interests.

Supplementary information

Table S1. List of InXTH candidate genes identified in the Ipomoea nil genome database (Asagao1.2).

Table S2. List of InXTH candidate genes identified in the NCBI GenBank database.

Table S3. Hub genes identified in the five key co-expression modules based on module membership (kME > 0.8) and expression levels.

Figure S1. Hierarchical clustering dendrogram of expressed genes identified by WGCNA.

Figure S2. Gene Ontology (GO) enrichment analysis of the co-expression modules.

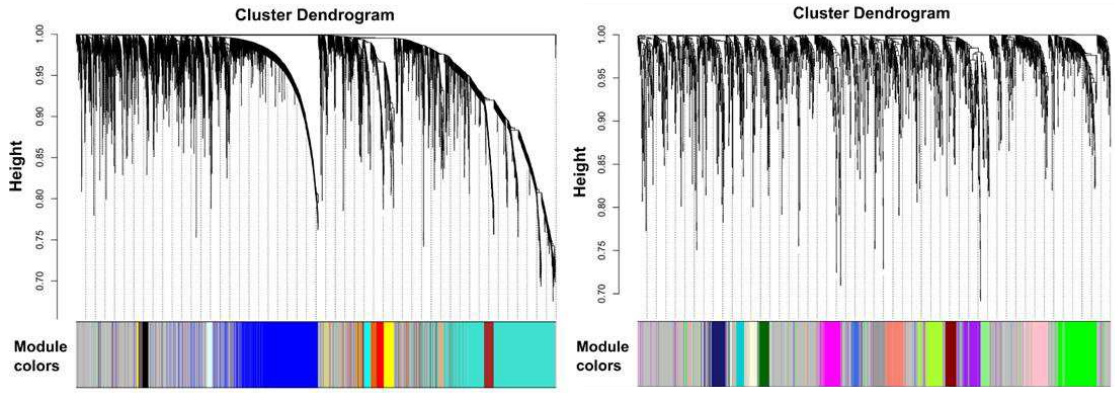

Supp Figure S1. Hierarchical clustering dendrogram of expressed genes identified by WGCNA.

The dendrogram was constructed based on the co-expression similarity (topological overlap) of expressed genes across the developmental stages of *I. nil* petals. Each vertical branch (leaf) in the tree represents an individual gene. The colored row below the dendrogram indicates the specific co-expression module to which each gene was assigned by the dynamic tree cut algorithm.

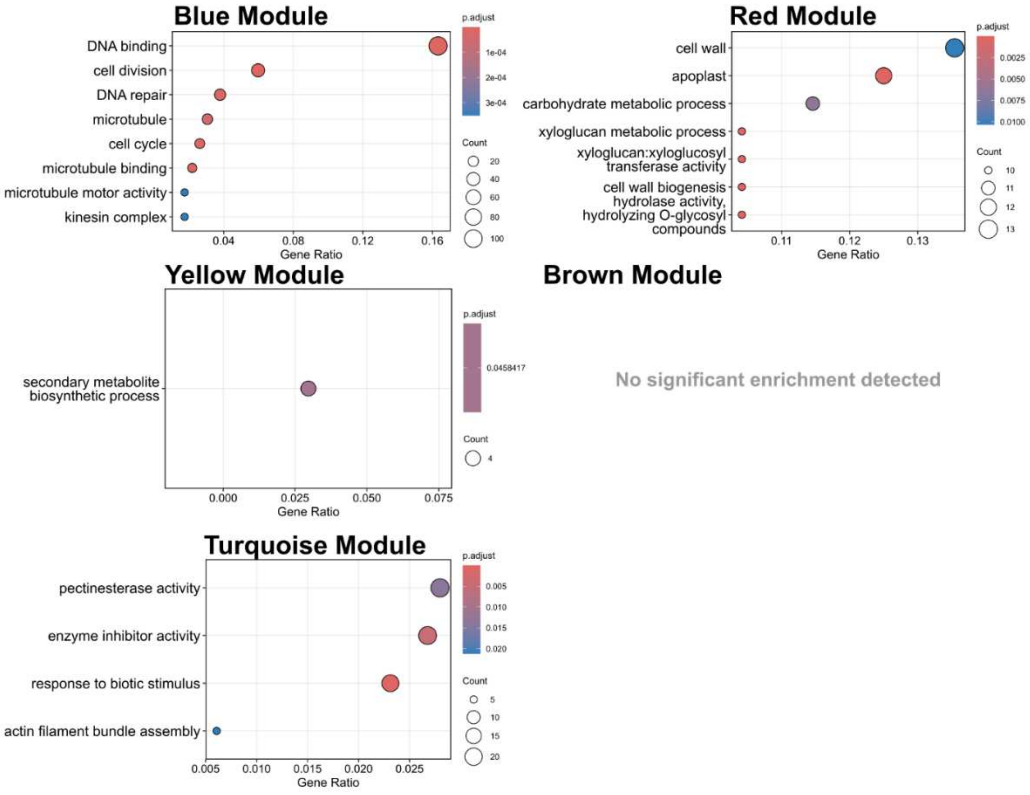

739

740 **Supp Figure S2. Gene Ontology (GO) enrichment analysis of the co-expression modules.**
741 Dot plots showing the top significantly enriched GO terms for the genes assigned to the blue, red,
742 yellow, turquoise, and brown modules identified by WGCNA. The enrichment analysis was
743 performed using the clusterProfiler R package based on a custom gene-to-GO term mapping
744 dataset. To ensure analytical accuracy, obsolete GO terms were excluded using the GO.db package
745 prior to the enrichment test. All genes filtered for the WGCNA were used as the background
746 universe. The statistical significance of enrichment was defined by a Benjamini-Hochberg (BH)
747 adjusted P-value < 0.05. The color gradient of the dots represents the adjusted P-value, while the
748 size of the dots corresponds to the number of genes (Count) associated with each GO term. The
749 x-axis indicates the GeneRatio (the proportion of module genes associated with a specific term
750 relative to the total number of annotated genes in that module). Note that no significantly enriched
751 GO terms were detected for the brown module.